Eivind Berg Rønning

Influence of site, turbine height and wind direction on the performance of vertical-axis wind turbines on model buildings

Master's thesis in Mechanical Engineering
Supervisor: Tania Bracchi
Co-supervisor: Yannick Jooss
June 2021

Master's thesis

◻ NTNU
Norwegian University of
Science and Technology

Eivind Berg Rønning

Influence of site, turbine height and wind direction on the performance of vertical-axis wind turbines on model buildings

Master's thesis in Mechanical Engineering
Supervisor: Tania Bracchi
Co-supervisor: Yannick Jooss
June 2021

Norwegian University of Science and Technology
Faculty of Engineering
Department of Energy and Process Engineering

NTNU
Norwegian University of
Science and Technology

Problem description

An experimental study will be carried out in the wind tunnel on a Savonius vertical-axis wind turbine (VAWT) to assess the wind resource in a built environment. The thesis is based on a previous study that examined the flow field over two cubes, acting as buildings, with particle image velocimetry (PIV) measurements. They found the wind turbine performance at six stream-wise locations on the roof for a fixed wind direction. However, since the flow in the urban environment is highly affected by local building geometries and the wind direction is arbitrary, the available power in the wind is expected to be orientation dependent. Thus, to obtain a better estimate of the wind resource for this particular environment, the present study will expose the turbine to different wind directions. The aim is to find the ideal site to place the turbine and investigate the influence of an adjacent cube.

Sammendrag

Vindturbiner som opererer i det bygde miljøet er utsatt for lavere gjennomsnittshastigheter og høyere turbulente svingninger enn i åpent terreng. Likevel er det regioner rundt bygninger der strømmen blir akselerert og hvor det kan være gunstig å plassere en vindturbin. I dette arbeidet er en Savonius vind-turbin plassert i et modellert bymiljø bestående av et kunstig gulv og to veggmonterte kuber med avstand på to kubehøyder, 2H. En parametrisk studie utføres for å bestemme idealposisjonen for å høste energi uavhengig av vindretningen. Dette gjøres ved å undersøke hvilken innvirkning ulike tilførselsvinkler har på effekten når to turbiner som er forhøyet forskjellig, er plassert i tre posisjoner på taket. Effekten beregnes ved å innhente data på estimert mekanisk dreiemoment og rotasjonshastighet. Det oppnås full effektkurver for fem innstrømningsvinkler, og enkeltoperasjonsmålinger utføres for finere diskretisering med tretten innstrømningsvinkler. Basert på gjennomsnittseffekten som er anskaffet over en full rotasjon, er det vist at midten på taket er det ideelle stedet å plassere den høyeste forhøyede turbinen som er undersøkt, og som spenner over $1.16 \leq z/H \leq 1.48$, hvor z er høyden målt fra kunstgulvet. Gjennomsnittlig effektutbytte er omtrent 20% høyere enn effekten i en ren strøm uten kubene i denne posisjonen. Effekten er vist å være sensitiv til turbinhøyder, og den nedre monterte turbinen er mindre effektiv. Det observeres videre at nabokuben har en betydelig innvirkning på effekten som ekstraheres av turbinen på taket.

Acknowledgements

Preface

The work is presented in article format. The master's thesis follows up on an existing campaign at the Norwegian University of Science and Technology (NTNU) that aims to explore the wind energy potential in the urban environment.

Contents

List of figures

List of tables

Influence of site, turbine height and wind direction on the performance of vertical-axis wind turbines on model buildings

Eivind Berg Rønning[1]

[1]Norwegian University of Science and Technology, Department of Energy and Process Engineering

June 18, 2021

Abstract

Wind turbines operating in the built environment are exposed to lower mean velocities and higher turbulent fluctuations than in open terrain. Still, there are regions around buildings where the flow is accelerated and where siting a wind turbine can be favourable. In this work, a wind turbine of the Savonius type is placed in a modeled urban environment consisting of an artificial floor and two wall-mounted cubes with a spacing of two cube heights, $2H$. A parametric study is carried out to determine the ideal position to harvest energy independent of the wind direction. This is done by investigating the impact various inflow angles has on the power when two turbines that are elevated differently are sited in three positions. The power is calculated by acquiring data on the estimated mechanical torque and the rotational velocity. Full power curves are acquired for five inflow angles and single operation point measurements are conducted for the finer discretization with thirteen inflow angles. Based on the average power acquired over a full rotation, it is shown that the central position on the roof is the ideal location to site the highest elevated turbine examined, spanning $1.16 \leq z/H \leq 1.48$, where z is the height from the artificial floor. The average power yield is about 20% higher than the power in a clean flow without the cubes at this position. The power is shown sensitive to turbine elevations, and the lower mounted turbine is less efficient. It is further observed that the neighbouring cube has a substantial effect on the power extracted by the wind turbines.

1 Introduction

Small wind turbines (SWTs) placed in the urban environment have experienced increasingly more attention (Bukala et al., 2015; Grieser et al., 2015; Vilar et al., 2020). Due to advancements in technology, efficient SWTs sited in the urban environment can realistically justify the investments over the long-term (Amer et al., 2021). Urban wind addresses the importance of utilizing local renewable energy resources, accelerating the transition to reduce carbon emissions in populated areas as a response to the worlds urgency for greener cities (see e.g. Agenda 2030 (Colglazier, 2015)). Advantages on building-integrated SWTs are summarized by Toja-Silva et al. (2013) and Stathopoulos et al. (2018) and it is likely that on-site wind energy generation ensures sustainable development assisting the distributed power generation in populated areas and simultaneously lower the energy losses related to electricity transport and construction and maintenance of massive transmission infrastructure.

Typically, turbines in the urban environment are installed in the region characterized as the roughness layer by Oke (1988). This sub-layer is situated from the top surface of the building up to roughly two to five building heights (Raupach et al., 1991). The flow in this region is highly affected by local building geometries and sizes. Unlike flow over open terrain, urban wind is characterized by high turbulence and low mean velocities (Ledo et al., 2011), making a general evaluation of the wind resources challenging. Nevertheless, regions with accelerated flow have been detected, usually over roofs and around buildings

for which placing turbines is significantly favourable for energy harvesting (Lu and Ip (2009); Ledo et al. (2011)).

It is common to investigate wind energy problems with computational fluid dynamics (CFD). Particularly wind exploitation on roofs is of interest (Mertens, 2003; Ledo et al., 2011; Abohela et al., 2013; Wang et al., 2017), and the flow fields are usually solved with the Reynolds-Averaged-Navier-Stokes (RANS) equations. In the numerical study by (Ledo et al., 2011) on flow over urban environments, they found that turbulence is strongly dependent on the wind direction and the roof profiles. Out of three roof profiles considered, the flat roof configuration was shown to be more favourable for siting a wind turbine over the pitched and the pyramidal roof. Furthermore, CFD analyzes on wind turbines sited in a built environment were reviewed by Toja-Silva et al. (2013). They reported that vertical-axis wind-turbines (VAWTs) are preferable to the horizontal-axis wind-turbines (HAWTs) in urban areas under multi-directional wind conditions. VAWTs have simple and solid structure, low noise emissions and they are capable of utilizing the wind without the need of yawing.

Abohela et al. (2013) conducted a study on different roof configurations on an isolated building, with the aim of finding the optimum roof from an energy-harvesting point-of-view. Six roof were investigated and for all cases, the maximum turbulence intensity (TI) reported was located below $1.3H$ above the rooftop, where H denotes the height of the isolated building. This in turn gave reason to recommend future turbine siting above this threshold. Similar height constraints were confirmed on flat roofs by Toja-Silva et al. (2015). They found that regardless of wind direction, HAWTs should be placed above $1.31H$ to be within the threshold of $TI = 0.15$ in compliance with the European Wind Turbine Standards for SWTs (TI has been normalized with the free-stream velocity). However, siting the turbine at such heights will thereby efficiently make the buildings 30% taller which could be quite extreme and non-trivial from a structural perspective. On the other hand, VAWTs were deemed more suitable closer to the roof since they could withstand greater levels of turbulence intensities and they are less affected by fluctuations in wind directions (Kooiman and Tullis, 2010; Mertens et al., 2003; Kooiman and Tullis, 2010). Moreover, Savonius wind turbines rotate relatively slow and they are considered practical in populated areas since noise emissions are proportional to the tip-speed U_{tip}^5 (the local velocity at the tip of the blades) (Burton et al., 2001). In addition, in terms of safety features and practical aspects, the generator and the alternator can be placed on the ground, which makes them safer to operate and easier to maintain and the risk of property damages is significantly lower than that of high-elevated fast-rotating HAWTs.

Research considering experimental data are more limited. Since numerical simulations are sensitive to modeling parameters (Stathopoulos et al., 2018), they need validation either through on-site field measurements or wind tunnel measurements. The former is suggested for utility-scale applications but they are quite hard to access. Nonetheless, wind tunnel data have been compared with field measurements and are demonstrated to be a valuable tool for the estimation of wind energy potential (Al-Quraan et al., 2016). Results showed that having a relatively homogeneous upstream terrain results in good agreement with field measurements with an error in estimated energy of 5%. Increasing the complexity of the upstream flow leads to increased uncertainty, however, still deemed acceptable for initial evaluations having maximum errors of 20% (Al-Quraan et al., 2016).

Flow over a high-rise building was investigated in a wind tunnel by Hemida et al. (2020) and amongst many conclusions, they reported similar behaviour and flow pattern to that of flow over lower-rise buildings. Moreover, Šarkić Glumac et al. (2018) studied a group of five similar-sized high-rise rectangular prisms acting as buildings in a cross-formation. From this, they investigated the flow as well as surface pressure on the centered building to analyze the wind-effects it will undergo when placed in the wake of the adjacent buildings for several incident angles of the incoming wind. It was found that 0° was the worst configuration for wind energy harvesting. This was due to high turbulence intensities in the wake caused by the presence of the upstream building. 45° was reported as the preferable orientation, resulting in a 25% amplification in the mean stream-wise velocity and multiple favourable turbine sites available at lower heights over the examined roof.

Even though wind resource assessment over buildings has been studied experimentally, they are commonly based on flow-fields instead of the performance-data extracted by a turbine which is shown to be rather different (Jooss et al., 2021). A more accurate measure would therefore be to include the turbines as they disturb the surrounding flow field when they extract energy and exert forces. Ge et al. (2021) reported that the turbine in the wake of a cubed-shaped building influences the performance of

a consecutive turbine farther downstream by the use of actuator disks. Even though such disks are of importance for wind resource evaluation, they are not quite representative of a realistic model in the near wake (de Jong Helvig et al., 2021). A study that covered a realistic model was conducted by Lee et al. (2018) where a small VAWT of the Darreus type was situated on the roof of a building. It was found that higher turbulence intensities yield more power at low velocities, whereas the opposite occurs for higher velocities. They also concluded that the vertical wind-component normal to the wall have an impact on the performance of the turbine on the roof and reportedly 90% of the power is extracted when the vertical angle is less than 45°.

Nonetheless, Toja-Silva et al. (2018) reported that the amount of research in the literature that consider the use of wind turbines in an urban environment is scarce. To address this void, the present study will follow up on the study conducted by Jooss et al. (2021). They placed a Savonius turbine in a simple modeled urban environment (two cubes in line with each other) and measured its performance at six different streamwise locations on the roof. Moreover, the flow field was mapped thoroughly with Particle Image Velocimetry (PIV) measurements both with and without the turbine on top of the cubes as wind approached the cubes normal to the windward facade (0°). In the present study, we examine how the turbine performance is affected by other parameters such as: the turbine height above the modeled buildings, locations on the roof and the incoming wind direction. The obtained data will be used to draw conclusions on where to site the turbine to gain optimal energy harvesting and look at the effects of the adjacent building on the power performance. The set-up is specifically designed for this purpose, allowing the turbine to face different flows when varying the incoming wind direction. To pursue the same modeled urban environment as used by Jooss et al. (2021), the set-up consists of two cubes that are placed in a tandem arrangement, with two cubes-lengths H between them. This reference-length H denotes the cube height and is 99 mm. The upstream incoming flow field is uniform. It was employed rather than having the cubes submerged in an urban boundary layer since even an atmospheric boundary layer is quite arbitrary for which the shape usually does not match the well-used power-law (Wagner et al., 2009). An upstream uniform flow is not only more comparable with other studies, but also more easily reproduced. The influence of different inflow profiles introduces another parameter (Castro and Robins, 1977) and should be studied separately.

Flow over a cube is well-described by the existing literature, see e.g. (Castro and Robins, 1977; Ogawa et al., 1983; Richards et al., 2007; Hearst et al., 2016) and there are some cases of flow over two cubes with same spacing as this study (Martinuzzi and Havel, 2000, 2004; Jooss et al., 2021). A study that considers a similar uniform flow over a single wall-mounted cube is the paper by Castro and Robins (1977). They reported that for flow normal to the windward facade of the cube (0°) the flow is independent of the Reynolds numbers $Re_H = U_\infty H \rho / \mu$ for $Re_H > 3 \times 10^4$, where U_∞, ρ and μ are the free-stream velocity, density an the dynamic viscosity, respectively. Martinuzzi and Havel (2000) reported Reynolds independence in the range of $Re_H = 12000 - 40000$ on the flow over two equally-sized cubes with similar spacing as the present study.

A detailed explanation on the experimental procedure is given in section 2. In section 3, the flow field is discussed. The experimental results are shown in section 4, and the conclusions are presented in section 5.

2 Experimental procedure

2.1 Geometrical configuration

The experiments were carried out in an closed-loop, low-speed wind tunnel at the Norwegian University of Science and Technology in Trondheim, with a test section of the height, width, and length of 1.8 m, 2.7 m and 11.1 m, respectively. The inlet of the test section is located 4 m upstream of the acrylic plate presented in section-view in fig. 1. The illustration show two cubes that represents buildings that are fixed mounted on a 10 mm-thick round acrylic plate, acting as a false floor. This floor is centered and attached to the rotating stage on legs in the tunnel illustrated in fig. 1 and thereby elevated above the wind tunnel floor. The material of the cubes was Ebaboard 0600 which is a synthetic, post-cured board material on polyurethane base.

A coordinate system is given in fig. 1 and fig. 2. The origin is placed in the center at the front cube
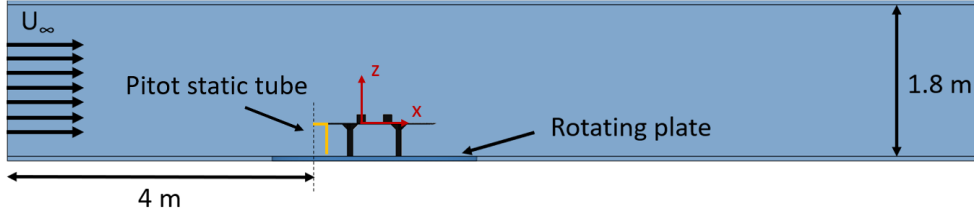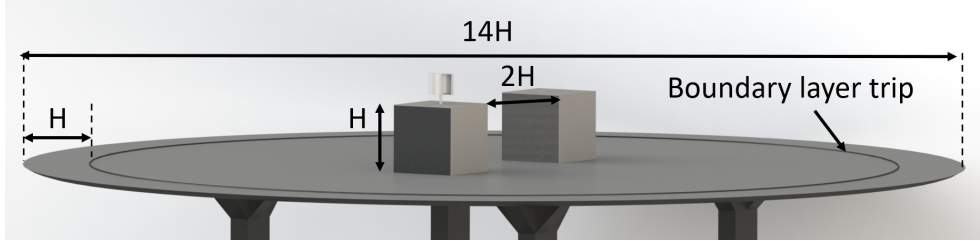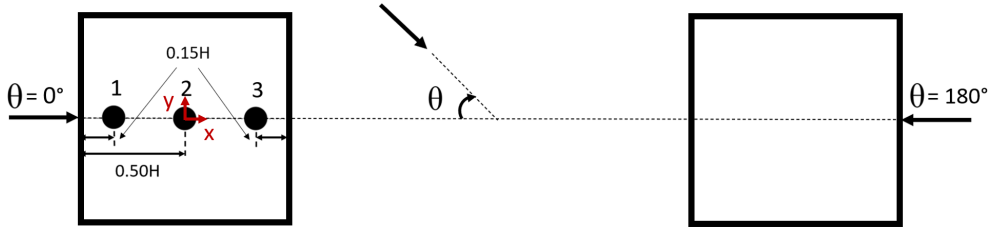
Figure 1: Side view of the experimental set-up in the wind tunnel. The origin is placed at the center of the front cube, on the artificial floor. The placement of the pitot-static tube is given in appendix (13(f)).

Figure 2: Illustration of the set-up. (a) Two surface-mounted cubes aligned and centered on the artificial floor. (b) Top view of the cubes. The numbering show the three turbine locations. θ is the incoming flow angle.

presented in fig. 1. Moreover, the coordinate-vector z is defined such that $z = 0$ at the plate's surface and is positive upward shown in fig. 1. The pitot static tube was placed in the height $z/H = 0$ and $x/H = -5.5$ next to the rotating stage to avoid flow obstructions and U_∞ was kept constant for all measurements yielding a Reynolds number of $Re_H \approx 6 \times 10^4$. To control the transition between laminar and turbulent flow, a round 2 mm-thick wire was used as a boundary layer trip that forced transition to a turbulent boundary layer as shown in fig. 2(a). Furthermore, the false floor is sharpened at the edge with a $15°$ angle to avoid flow separation of the incoming air. Whereas the paper by Jooss et al. (2021) considered six turbine positions on the roof, three on each cube, the present study only examine the foremost cube in fig. 2(b) since the system rotates and the model is symmetric. In that way, the front cube eventually becomes the back cube when the plate is yawed $\theta = 180°$. From now on, θ is referred to as the inflow angle and represents the wind direction. The three available positions for siting the turbines as well as the angle convention are presented in fig. 2(b). Performance measurements were carried out on two identical-shaped Savonius turbines identified as the *low* and the *high* turbine. They are only different in their tower heights placed above the modeled buildings with the blades sweeping between $z/H = 1.08 - 1.40$ and $z/H = 1.16 - 1.48$, respectively. The design of the Savonius turbine was chosen to be the exact same an in Jooss et al. (2021). They report that it was simple for manufacturing reasons and not optimized for energy extraction. Nevertheless, some general design decisions were taken from literature, such as including end-plates and having two-, rather than a three-buckets turbine. In addition, the overlap ratio o/D, where o is the distance of the bucket overlap and D is the diameter,

4

was chosen to acquire better aerodynamics and lower the starting torque. An illustration of the design is given in the appendix (see fig. 12). More on Savonius and design recommendations are found in Blackwell et al. (1977) and Akwa et al. (2012). With the initial aim to find the optimal turbine-site independent of the wind direction, wind from various directions have been considered. Therefore, power measurements were conducted for thirteen incoming flow angles with $15°$ steps ranging from $0° - 180°$. In addition, a total of one hundred pressure-taps were evenly distributed on the surfaces of the cubes to map the flow field. A pressure scanner of type $MPS4264$ was used for this purpose and the mean values were measured over 60 seconds at $800Hz$. More information about the flow field is described in section 3. As the plate changes orientation in the tunnel, it does not only introduce a change in the flow field seen by the turbine due to obstructions of the surroundings (here two modeled buildings), but it also introduces a change in the wind tunnel blockage, namely the frontal model area with respect to the cross-sectional area of the tunnel test-section. The blockage of the set-up was found below 5% at maximum, however, it was considerably lower for most cases. At Reynolds numbers of $Re_H \approx 10^4 - 10^5$, the blockage effects can be considered negligible (West and Apelt, 1982).

2.2   Wind power conversion

The performance of a wind turbine is compared with the power coefficient defined as the mechanical power extracted divided by the theoretical, maximal available power in the wind,

$$C_P = \frac{Q_{sh}\Omega}{\frac{1}{2}\rho A U_\infty^3}, \tag{1}$$

where the mechanical shaft torque is given as Q_{sh} and the rotational velocity is denoted Ω. Moreover, A is the cross-sectional area of the Savonius turbine, which is calculated by: $A = Dh$ where h is the turbine height. According to Manwell et al. (2010), the value of C_P is limited and can not go beyond 59.3%. However, this limit, called Betz' limit, is due to several assumptions that make it not quite reachable in reality. Full-scale modern conventional VAWTs achieve $C_P \approx 0.2-0.3$. However, this can not be expected for small-sized wind turbines due to scaling effects. It has been reported by Blackwell et al. (1977) that the Reynolds number has impact on the boundary layer separation that occurs on the convex side of the buckets where a delayed separation results in reduced pressure drag on the returning bucket which eventually gives more lift force. Thus, an increase in Reynolds number is expected to increase C_P and tip speed ratio: $\lambda = \Omega R/U_\infty$ where R is the radius of the turbine. Aliferis et al. (2019) showed this effect in their study on a helical two-bucket Savonius turbine. They reported that by increasing $Re_D = U_\infty D/\nu$, with rotor diameter as a reference, from 1.6×10^5 to 2.7×10^5, the measured power increased by 48% when the inflow turbulence intensity, TI, was fixed to 0.6 %. Other apparent Reynolds effects are observed in wind tunnels tests by Kooiman and Tullis (2010) and in numerical simulations by Akwa et al. (2012) and El-Askary et al. (2015). Moreover, it was shown that Reynolds number independency is not completely reached before $Re_D \approx 2 \times 10^5$ (El-Askary et al., 2015). Since the present study has a Reynolds number of $Re_D = 2.5 \times 10^4$, which is about an order of magnitude lower, an inevitable Reynolds effect is presumed in these experiments. In the prefatory stage, the effects were noticed and a study on the Reynolds dependence was carried out and can be seen in the appendix (12). Furthermore, Aliferis et al. (2019) observed that for low Reynolds numbers, there were no clear effects in the power performance by varying the free-stream turbulence from $TI = 0.6\%$ to 5.7%, and that suggests the performance of a scaled VAWT is relatively independent on fine changes in turbulence.

To measure the mechanical shaft torque Q_{sh} in (1) of a miniature wind turbine is quite difficult due to its low magnitude. Nonetheless, due to their size, a suitable way of calculating the mechanical power P indirectly was proposed by Bastankhah and Porté-Agel (2017). The illustration in fig. 3(a) was made with inspiration from their study. They used a similar procedure as Kang and Meneveau (2010) and measured P directly with a strain-gauge instrumented plate and compared it to the electromagnetic converted power P_{conv}. The relation between these power expressions is $P = P_{conv} + P_f$ illustrated in fig. 3(a), where P_f is the power related to the friction between the rotating armature and the air, in addition to the friction in the bearings (Chapman, 2005). It was shown that $P_{conv} = Q_{conv}\Omega$, is fairly close to P itself (Bastankhah and Porté-Agel, 2017). The converted electromagnetic torque is given by $Q_{conv} = k_M I$ (Hughes and Drury, 2019), where the measured armature current flowing in the circuit, I, is inversely proportional to Ω. The torque constant k_M is supplied by the manufacturer listed in table 1.
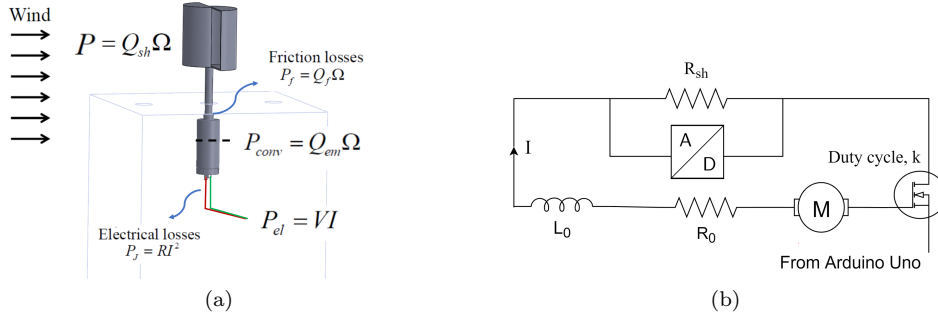
Figure 3: (a) Wind power conversion for a miniature Savonius turbine exposed to wind. (b) The electrical circuit of the system operating at duty-cycle, k.

Note from fig. 3(a) that $P_{conv} \neq P_{el}$ since the electrical power, P_{el}, represents the actual electric power generated by the permanent magnet direct current (PMDC) device. This quantity is largely affected by copper losses due to armature resistance and other losses related to core- and stray losses. The former can be expressed as $P_j = RI^2$, where R is the resistance coming from the armature and the field copper windings, not the external resistance (Chapman, 2005). Moreover, the friction torque Q_f decreases for lower speeds when a PMDC machine is used as a generator (Bastankhah and Porté-Agel, 2017). This implies that $P_f << P_{conv}$ for lower operating speeds.

2.3 Speed controller and data acquisition

A Metal–Oxide–Semiconductor Field-Effect Transistor (MOSFET) was connected in series with a brushed motor ($12G88$ Athlonix) used as a generator, as illustrated in fig. 3(b). Adapting a similar method that Gambuzza and Ganapathisubramani (2021) deployed in their experimental study of the effect of turbulence on the performance of a model wind turbine, the Pulse-Width-Modulation (PWM) technique controls the voltage fed to the load and thus indirectly the speed by rapidly switching between a closed and open circuit. The rate can be set as an analog value (PWM wave) ranging from 0 to 255 that controls the PMDC at various speeds. This switching rate will henceforth be referred to as duty-cycle k. Here, $k = 0$ means the circuit is closed and thereby no current will flow in the windings. This MOSFET device causes the current to average over a low impedance, yielding a low voltage drop and power dissipation.

The performance was mapped by changing duty-cycle operation points. That is, the amount of converted electromagnetic torque Q_{conv} at a respective rotational velocity Ω for a chosen switching rate k. To obtain Q_{conv}, the current was measured with an Adafruit INA219 sensor. This device is a 12 bit Analog-to-Digital converter (ADC) power monitor and a shunt resistor powered by the Arduino Uno micro-controller. The precision amplifier measures the voltage across the shunt resistor of 0.1 Ω, and the current is calculated by applying Ohm's law, $I = V/R_{sh}$. Here, V is the measured voltage, and R_{sh} is the shunt resistance. The expected maximum current output with the $12G88$ device is less than 400 mA for these experiments and the *Arduino* software was set to minimize the internal gain to boost the resolution to ± 0.1 mV.

To acquire the rotational velocity of the shaft, Ω, an optical encoder of model type OPB705WZ was coupled with the same Arduino board. It responds to illumination from the emitter when the reflective tape on the turbine passes within the field of view. Both I and Ω were collected individually with an external software called *CoolTerm* through a serial port with a baud rate of 9600 Hz. The sampling rates were approximately 200 Hz which was deemed sufficient since the maximum operational speed was not exceeding 3600 RPM = 60 Hz and the rotational signal is said to be free of distortion when the sample-rate is greater than twice the size of the highest frequency represented in the signal (Landau, 1967).

6

Table 1: Generator characteristics

Electrical Data	*****	DC Machine 12G88 Athlonix	Units
Torque constant	k_M	4.90	mNm/A
No-Load Speed	n_0	8670	RPM
No-Load Current	I_0	16.00	mA
Terminal Resistance	R_0	3.20	Ω
Max Continuous speed	n_{max}	12000	RPM
Max Continous current	I_{max}	730	mA
Max Continous torque	Q_{max}	3.50	mNm
Friction Torque	T_f	0.08	mNm
Rotor Inductance	L_0	0.08	mH

2.4 Measurement uncertainties

An uncertainty analysis including both systematic and random errors based on Wheeler and Ganji (1996) was carried out for the measurements, which is described in more detail in the appendix (A.3). The uncertainties of C_P and λ are calculated for a 95% confidence interval. As for the equipment where the confidence interval is not specified, assumptions are made so that the total error for each variable is derived from the root sum square of the biased and random errors. The maximum errors of C_P and λ were found to be less than 3.5% and 1.5%, respectively. In the following, all performance plots are given with error bars.

3 Baseflow field

A turbulent boundary layer profile was obtained by measuring the mean stream-wise velocity U when the cubes were removed and is illustrated in fig. 4. The boundary layer thickness was found to be $\delta/H = 0.32$ thus the inflow can be classified as uniform. While the turbulence intensity in the free-stream was found to be about 1% based on hot-wire measurements from a previous study conducted in the same tunnel (Cantan, 2021), the flow over the cubes on the other hand, is highly turbulent (Martinuzzi and Havel, 2000, 2004; Hearst et al., 2016; Jooss et al., 2021). To obtain information on the flow at the surfaces of the cubes, the mean pressure was found with the pressure coefficient:

$$C_p = \frac{p_s - p_\infty}{\frac{1}{2}\rho U_\infty^2},$$

(2)

where p_s is the static pressure and p_∞ and U_∞ is the pressure and velocity in the free-stream when the cubes are removed from the tunnel, respectively. The pressure distribution over the upstream cube for an inflow at $\theta = 0°$ is presented in fig. 5. The pressure is plotted along three lines; center ($y/H = 0$) and $y/H = \pm0.35$, together with data from Castro and Robins (1977). The latter considered two flow-cases; a thin and a thick boundary layer corresponding to an upstream uniform flow similar to the one
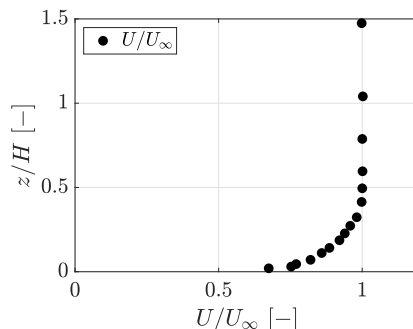

Figure 4: Stream-wise velocity normalised by U_∞ measured on the artificial floor.

in this study and an atmospheric boundary-layer flow where the cube is fully immersed, respectively. From the obtained data points, the pressure over the roof is in good agreement with the uniform inflow case, and unlike the boundary layer flow, the pressure does not drop over the surface. This finding demonstrates that the shear layer separating from the leading edge does not reattach further downstream over the investigated cube (Castro and Robins, 1977). The stagnation point was found at $z/H = 0.60$ to be $C_p = 0.85$ on the windward facade, whereas Castro and Robins (1977) reported a maximum at $z/H = 0.45$ having $C_p = 0.99$. However, here, the pressure is taken with a coarse discretization; thus the location of the stagnation can only be determined with an accuracy of $z/H \approx \pm 0.2$. Moreover, when comparing the pressure on the windward facade, the huge discrepancies observed are likely due to different boundary layer thicknesses δ/H where a horseshoe vortex typically forms (Martinuzzi and Havel, 2004). In fig. 6 the velocities obtained by Castro and Robins (1977) at the center of the roof is mapped together with the blade swept area of the *low* and the *high* turbine. As shown, the flow field is quite different over the cubes when the inflow angle is changed.
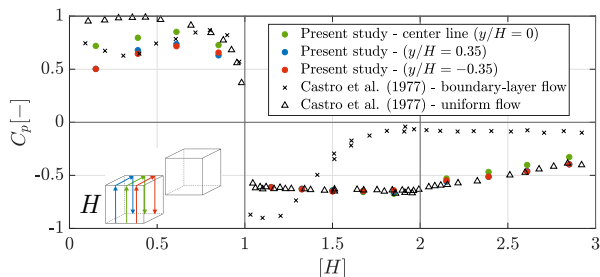

Figure 5: At inflow angle $\theta = 0°$, the mean surface pressure coefficient C_p is plotted along three lines on the front cube together with data from Castro and Robins (1977) (marked black) along the center-line $y/H = 0$.
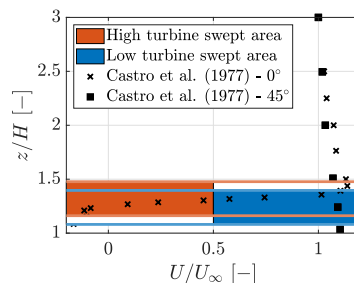

Figure 6: The blade swept area A of the *low* and *high* turbine together with the mean stream-wise velocities measured at the center of the cube ($x/H = y/H = 0$) obtained by Castro and Robins (1977). The color-lines are a continuation of the swept area.

Fig. 7 shows surface pressure over the white roof presented down in the right corner for five wind directions without the turbine. As the wind direction switched to $\theta = 45°$, two distinct suction regions are formed on each of the sweptback leading edges, and an abrupt increase in pressure takes place farther downstream. Such a pattern is well documented in the literature (see e.g. Lin et al. (1995); Banks et al. (2000); Franchini et al. (2005)). Those studies illustrate two conical vortices over the roof, associated with each edge. Moreover, at $\theta = 45°$, as the pronounced regions occurring are not symmetrical, it is unclear whether this comes from uneven-sharpened edges or a small misalignment with the incoming flow. The latter was investigated in the tunnel by fine tuning the angle and it was found that pressure is quite sensitive to the angle of the incoming flow. Still, pressure fields between $0°$ and $180°$ are symmetric, and it would seem that the former is the case here. At $\theta = 135°$ the conical structures at the edges are less prominent compared to $\theta = 45°$, which could be explained as a result of the building being embedded in an urban environment (Case and Isyumov, 1998). Moreover, studying the pressure field when the flow approach at $90°$, an asymmetric pressure distribution arise solely due to the influence of the neighbouring cube. The distinct lower pressure at the edge indicates a "Venturi-effect" (Blocken et al., 2008) which is a result of the Bernoulli's principle. The flow is expected to accelerate in such a setting and greater velocities are expected here. Another remark worth noticing is the differences in the pressure as the wind comes from $180°$ rather than that of $0°$, which is purely due to the cube being situated in the wake of the neighbouring cube.
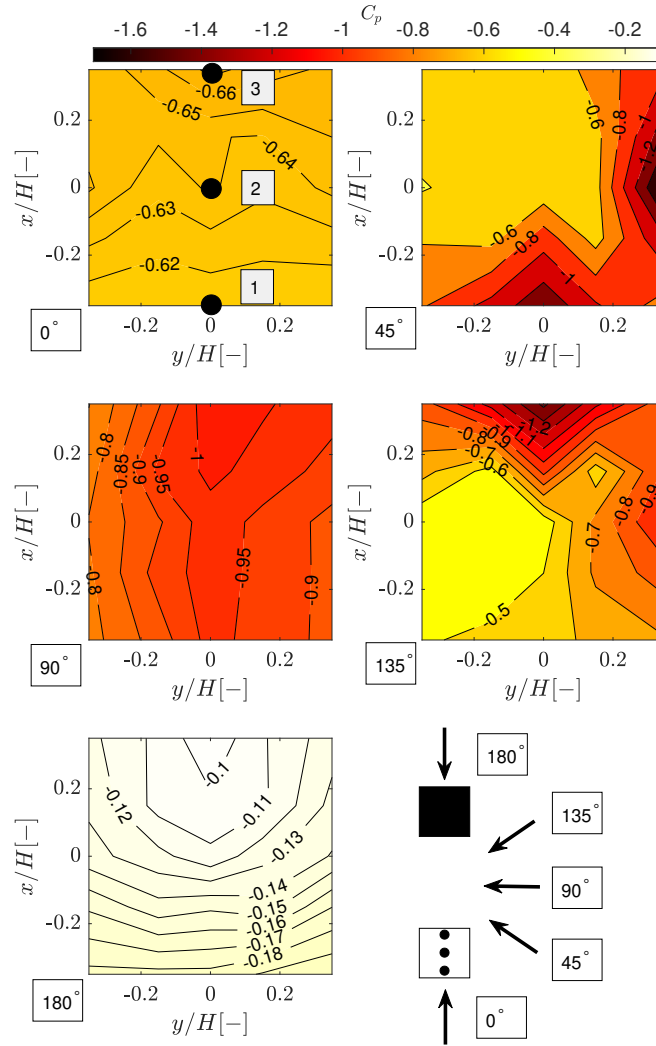
Figure 7: Mean surface pressure coefficient over the roof of the investigated building (the white one in the figure) for different inflow angles when the turbine is not present. The arrows show the approaching wind directions and the three black dots represent the turbine positions.

4 Wind turbine results and discussion

4.1 Clean flow

A benchmark-test of the turbine performance was carried out in free-stream conditions when the cubes were removed. The two Savonius turbines of different stand-off height are evaluated to indicate gains and losses that are expected when the turbines are situated on the roof later on. Small disturbances originating from the tower beneath the turbines are acknowledged, still these measurements provide a good reference of the turbine energy production in the absence of the cubes. Since the flow is not quite uniform it is henceforth classified as "clean air". The coefficient of power C_P and torque ($C_{Q_{sh}} = C_P/\lambda$) are presented with respect to tip-speed ratio in fig. 8a) and fig. 8b), respectively. All the measurements were taken at $x/H = 0, y/H = 0$ and same distance z/H above ground as for the measurements with the cubes. The C_P measurements suggest the turbines are equally efficient for low values of λ, however a slightly improved performance is observed for the *low* turbine where the maximum power coefficient was found to be $C_{P_{ca}} \approx 0.042$ when $\lambda \approx 0.35$ which is 2% higher than $C_{P_{ca}}$ of the *high* turbine. This is

9

within the measurement uncertainty. It can be observed that for further increased tip speed ratios the *high* turbine performs slightly better than the *low* turbine. A coarse discretization like here may not provide an exact shape, however, a slight kink around $\lambda = 0.6$ is visible in fig. 8. Similar kinks are found in Akwa et al. (2012); El-Askary et al. (2015); Mohamed et al. (2011); Aliferis et al. (2019). It should not be excluded that the surface roughness on the turbines are printer-determined which may result in friction drag differences, however, the printer comes with great accuracy (20 micron in layer resolution see Ultimaker), thus the more likely explanation is the impact of the tower below which affects the turbines of different heights differently.
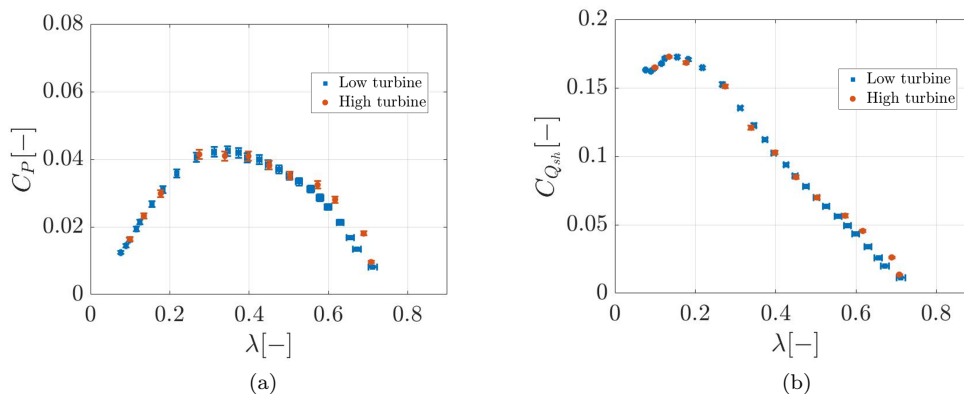

Figure 8: A benchmark test for the turbine performance in "clean air". (a) Power coefficient over tip-speed ratio. (b) Torque coefficient over tip-speed ratio.

4.2 Influence of inflow angle, height and position

The goal of this study is to determine the influence of wind direction and siting on the performance of a VAWT on model buildings. This was studied parametrically by varying the inflow angle as well as position and height of the turbine. Various power curves for five inflow angles in each of the three examined positions are presented in fig. 9. The surface pressure on the buildings for these inflow angles was discussed in fig. 7. In addition, data on the maximum performance $C_{P_{max}}$ and the corresponding tip-speed ratio λ are reported and summarized in table 2 for a better overview. For more information on the positions and the angle convention, a graphical explanation is presented in fig. 2. The overall power evaluation indicates that the performance is highly orientation-dependent and there are significant variations between the turbine heights where in particular the *high* turbine is showing promising performance over the roof. Poor turbine performance (here $\theta = 0°$ and $\theta = 180°$) can be explained with the separation bubble occurring at the leading edge of the foremost cube that increases in height over the roof, covering a wide region of re-circulation farther downstream. In this region, the flow is highly turbulent and has lower stream-vise mean velocities (see e.g. the flow pattern in Martinuzzi and Havel (2004) and Jooss et al. (2021)). Both turbines show their poorest performance when the cube they are positioned on is in the wake of the upstream cube ($\theta = 180°$). This configuration can be classified as "worst-case", as reported by Šarkić Glumac et al. (2018).

As $\theta = 0°$, it is observed that the turbine height matters to an extent that almost no power is utilized when the *low* turbine is sited at position 2, while the *high* turbine shows approximately 17% better performance than that of the "clean air" reference-test ($C_{P_{ca}}$) in the same position. This is a remarkable increase in power which could be explained by looking at the PIV measurements in Jooss et al. (2021) where the height of the separation bubble is quite distinct and the *low* turbine is almost fully immersed. This can be similarly observed in the flow field obtained by Castro and Robins (1977), sketched in fig. 6. Here, the *low* turbine does not span the accelerated flow region and is rather situated beneath in the territory highly influenced by reversed flow.

In all positions examined, both turbines extract more energy when $\theta = 0°$ compared to $\theta = 180°$, except the *low* turbine in position 3. From Jooss et al. (2021) it can be seen that the turbine, equally
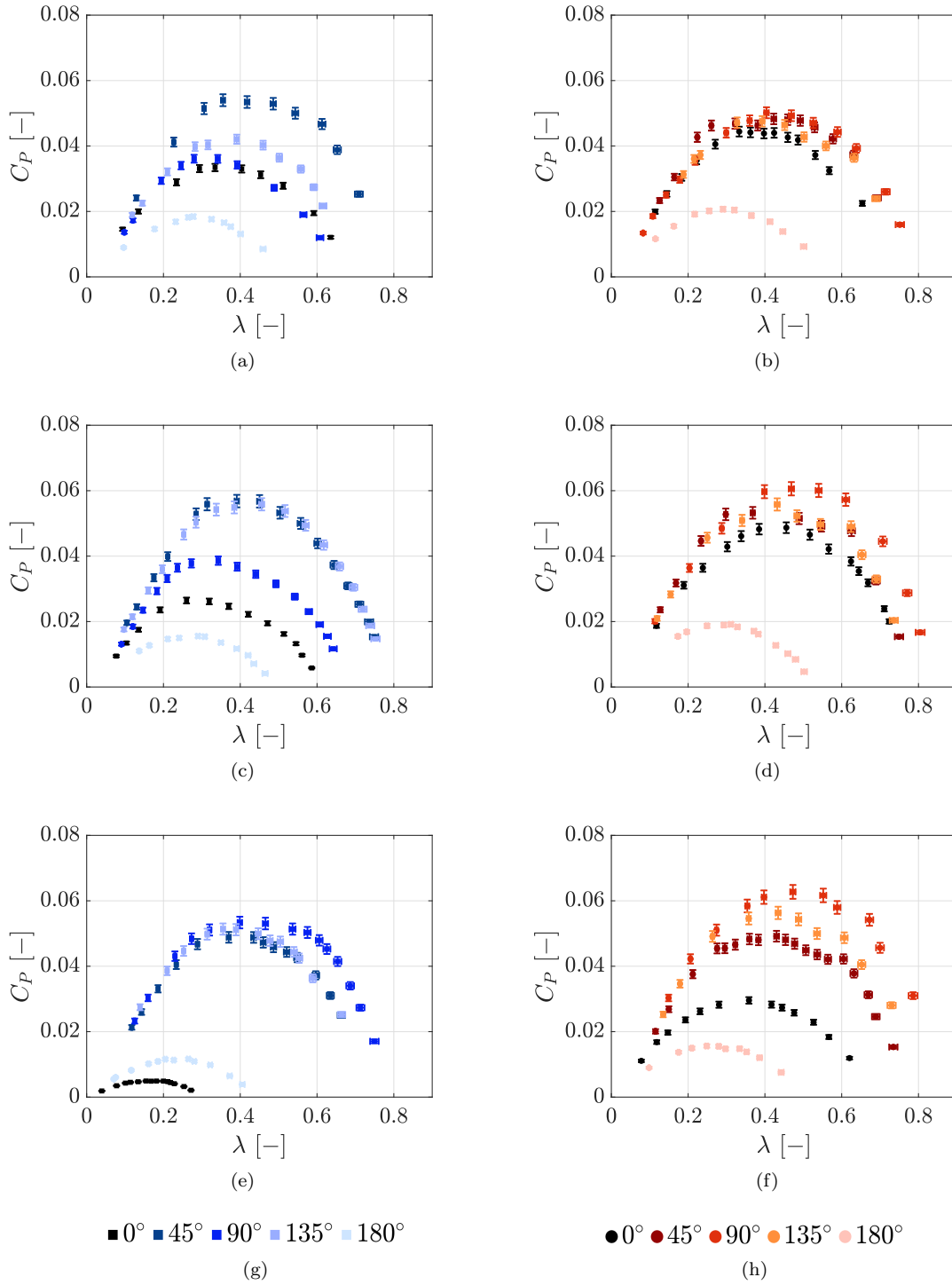
Figure 9: Power coefficient over tip speed ratio for the *low* and the *high* turbine on the left and the right column, respectively. (*a*) and (*b*) - Position 1. (*c*) and (*d*) - Position 2. (*e*) and (*f*) - Position 3. (*g*) and (*h*) - θ (see fig. 2(*b*).)

elevated as the *low* turbine in the present study, is almost fully immersed in the recirculation-bubble when sited at the far back. This result insinuates that increasing the turbine height further could potentially yield a better power output. Still, how much of an advantage it is by elevating the turbine further is

quite challenging to appraise with the limited data in the flow field and also the fact that they are not practical to realise in the real world. There are, however, some wind angles that are more favourable for the lower turbine compared to the *high* turbine. For instance, it was found optimal for $\theta = 45°$ and $135°$ where the maximum power coefficients are higher or about equal to the values of the *high* turbine, reported in table 2. A reason for such results could possibly be that the maximum velocities are formed closer to the surface, (see $\theta = 45°$ in fig. 6) which would explain why the turbine at low heights performs remarkably well in this region.

A question that was left open for discussion back in the introduction is the influence of the neighbouring building on the power extracted by the turbines. A method to highlight the significance of an adjacent cube's presence is to analyze the impact different wind directions in table 2 can have on the turbine performance. To quantify this, a reference was set and is described in the following. As $\theta = 0°$, by assuming the flow over the roof on the upstream cube is unaffected by the cube situated downstream, the turbine on the front cube yield as if the downstream cube is removed from the tunnel. This assumption might not be that restrictive considering that Jooss et al. (2021) found the upstream flow to be what influences the performance. Moreover, since the adjacent cube is removed in theory, the performance at the centered position (denoted position 2) would yield the same result as if flow approaches the cube at $\theta = 90°$ and $180°$, due to symmetry (Abohela et al., 2013). Therefore, by taking the aforementioned unknown error with caution, the neighbouring cube's influence on the turbine placed in position 2 have been estimated by analyzing the power differences: $\Delta C_{P_{90}} = C_{P_{max}}(\theta = 90°)/C_{P_{max}}(\theta = 0°)$ and $\Delta C_{P_{180}} = C_{P_{max}}(\theta = 180°)/C_{P_{max}}(\theta = 0°)$, when the wind approaches from $\theta = 90°$ and $180°$, respectively. Here $C_{P_{max}}(\theta = 0°)$ is the reference-power in position 2. For the *low* and the *high* turbine, the extra amount of extracted power when the wind approaches $90°$ are $\Delta C_{P_{90}} = 50\%$ and 25%, respectively. Since the additional power-gain is solely due to the existence of a neighbouring building, such findings elucidate the importance of the surroundings when a turbine is placed in the roughness sub-layer. Moreover, there are conceivably bigger differences in position 3 since it is situated closer to the neighbouring cube. This is also visible in the pressure field in fig. 7 and it seems to occur greater velocities in the passage at this inflow angle. As $\theta = 180°$, the loss in power with respect to inflow at $\theta = 0°$ was found to be $\Delta C_{P_{180}} = 39\%$ and 61% for the *low* and the *high* turbine, respectively. Hence, due to the adjacent cube's presence, there are huge gains and losses in power on the roof and it depends on what perspective one chooses to present. The orientational disparities shown in the power underline the necessity of including a broader span of inflow angles to assess a realistic optimal turbine position over the roof. Abohela et al. (2013) examined this over an isolated cube with a flat roof geometry by evaluating the wind velocities over a full rotation. They reported for a coarse angle step of $45°$ (like fig. 9), that the favourable wind conditions occurred when $\theta = 45°$ and the optimum location to mount a wind turbine was proposed, in this case, somewhere in between position 1 and position 2. However, it would likely be different when having a finer angle-increment since Wang (2020) found the favourable wind direction over a flat roof to be $60°$ when he considered a $15°$-increment. In the following chapter, the optimal site is investigated by calculating the average of all the measured wind directions, $\overline{C_P}$, rather than draw conclusions on preferable wind directions.

Table 2: Summarized performance data on the comparison between the *low* and *high* turbine at five inflow angles in three position. Relative power was calculated based on the maximum performance in the "clean air" benchmark test, $C_{P_{ca}}$. Green and red colors denoting gains and losses, respectively. The biggest power-gain is marked dark-green for both turbine heights. Note that from fig. 8, the value of $C_{P_{ac}}$ is different for the *low* and the *high* turbine and they are both used below as reference. Here, λ is the corresponding tip-speed ratio to the maximum power coefficient $C_{P_{max}}$.

| Angle	Site	Low turbine			High turbine		
θ	Position	$C_{P_{max}}$	λ	$(C_{P_{max}}/C_{P_{ca}}) - 1$	$C_{P_{max}}$	λ	$(C_{P_{max}}/C_{P_{ca}}) - 1$
	1	0.033	0.334	-21.2%	0.044	0.333	7.1%
$0°$	2	0.026	0.260	-37.7%	0.049	0.456	17.4%
	3	0.005	0.155	-88.4%	0.030	0.359	-28.7%
	1	0.054	0.355	27.3%	0.048	0.423	16.5%
$45°$	2	0.057	0.391	34.0%	0.053	0.368	28.4%
	3	0.049	0.370	15.1%	0.049	0.430	18.6%
	1	0.036	0.280	-14.9%	0.050	0.404	21.0%
$90°$	2	0.039	0.343	-9.0%	0.061	0.469	46.1%
	3	0.053	0.399	26.1%	0.063	0.473	51.3%
	1	0.042	0.391	-0.8%	0.048	0.393	14.7%
$135°$	2	0.056	0.456	31.7%	0.056	0.432	34.6%
	3	0.051	0.355	21.0%	0.056	0.434	35.8%
	1	0.018	0.278	-56.6%	0.021	0.291	-50.1%
$180°$	2	0.016	0.290	-63.2%	0.019	0.311	-53.8%
	3	0.012	0.265	-72.6%	0.016	0.249	-62.3%

4.3 Angle sweep
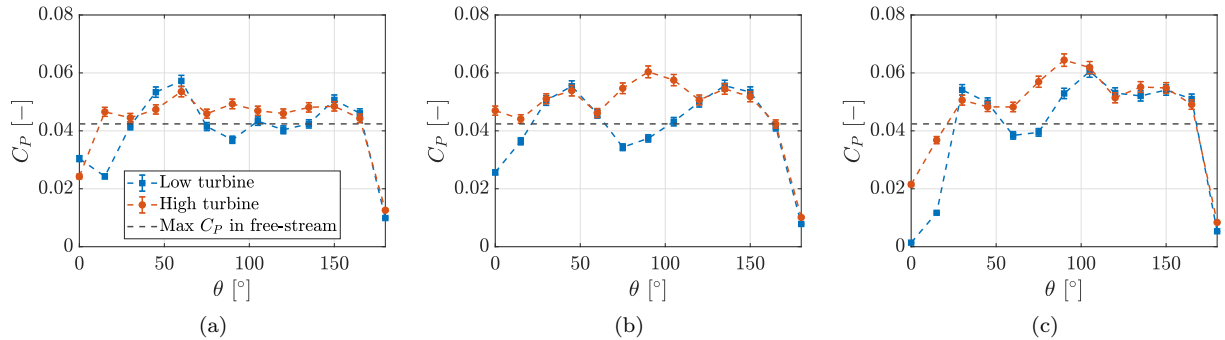
Figure 10: Performance measurements over the inflow angle. The data points are obtained with a fixed duty-cycle, $k = 200$. Axes are equal for all plots. (a) - Position 1. (b) - Position 2. (c) - Position 3.

The turbine positions were further examined with a finer inflow angle discretization while the turbine operated at near-optimum performance. It was attempted to measure the power peaks with two separate approaches; fixing the duty-cycle k and fixing the tip-speed ratio λ with less than 3% error of the mean. The latter approach was deemed insufficient because it lead to jumping from λ lower than λ^*, to higher, depending on the inflow angle θ. Here, λ^* denotes the tip-speed ratio corresponding to the maximum power coefficient $C_{P_{max}}$ at a given θ. Since these results are a bit ambiguous, they are presented in the appendix (A.1) and will not be discussed further. Considering the former approach, preliminary work gave insight and concluded that most power-peaks are found as duty-cycle $k = 200$ and that the overall $C_{P_{max}}$ occurred at this duty-cycle (see section 2.3 for more information on k). In addition, unlike the fixed-λ approach, the acquired data are located on one side of the $C_P - \lambda$ curves rather than jumping

13

around.

The value of C_P is mapped for the different wind directions in fig. 10. The angle sweep data was compared to the performance curves in fig. 9 and the points in $\theta = 45°$, $90°$ and $135°$ were found to be in good agreement with the peaks having less than 3% error for both turbines and the discrepancies were within the total uncertainty-limits in the power measurements (see A.3). The accuracy can be explained by the flat peak that is observed in the $C_P - \lambda$ curves, for which a small error in λ yield an inferior power output. On the other hand, the calculated maximum errors were significant when the wind directions were $\theta = 0°$ and $\theta = 180°$. They were found to be 71% and 54%, respectively.

An arbitrary fixed value of k, here chosen to be optimal for favourable wind conditions, are on the other hand, not up to standards for rather poor conditions. Keep in mind that the power (1), as well as the tip-speed ratio λ, are calculated based on the reference velocity U_∞ and not the local velocities over the roof. From the flow field in Jooss et al. (2021), it was observed that they are not the same thing. Hence, by varying the inflow angle, the $C_P - \lambda$ curve shifts depending on the flow seen by the turbine and this trend is visible in fig. 9. It is also expected Reynolds number effects that will affect the power outcome, however this order of significance has not been quantified in the results.

The aforementioned errors are therefore inevitable as this approach was implemented and the results are not quite optimal for all angles investigated in fig. 10. Still, only a few data points show worse performance than the dotted black line, $C_{P_{ca}}$, that represents maximum yield in "clean air" (see section 4.1). This is especially true for the *high* turbine. Moreover, in spite of the fact that some data measurements are worse than $C_{P_{max}}$, the trends can be expected to be conserved. Furthermore, the errors were exaggerated by highlighting the maximum differences, but they were usually lower. It is therefore believed the measurements are applicable for the thesis statement and have been considered in the site-analysis in table 3.

The data in table 3 considers three methods (A, B and C), which are evaluated in the examined turbine positions. Method A is the method that refers to the average maximum performance of all the inflow angles in the $C_P - \lambda$ curves in fig. 9. Method B takes the average of data points from fig. 10 and lastly, method C combine method A and B by taking the average of the maximum data-points by both.

There are some results that should be highlighted from table 3. Method B yields equally or better average performance for both turbines over method A in all the examined positions. Indeed, even though a few of the measured data-points in method B were less than optimal, the power extraction in the "worst case" wind directions ($\theta = 0°$ and $\theta = 180°$) are extremely influential on the average power due to their minimum yield. Hence, the significance of including 24 wind directions (due to symmetry), rather than 10 over the full rotation is quite distinct. Moreover, out of the three cases investigated, method C is the better representation on the average maximum power even though it realistically is not optimum since data points in B, as stated, were not optimum everywhere. Still, it has quite some advantage over method A and the average changes are given in table 3. The less influenced position is found to be at the center. At this location, the *high* turbine is only 5.7% more efficient when considering 24 inflow angles over the full rotation. Still, the average power-changes are likely to be huger in reality as more optimal points can be acquired. Note that the biggest changes in the average power are found to be 28.5% for the *low* turbine in position 3, whereas the higher turbine, also hugely influenced, have 17.2% additional power in the same position. This is likely due to the neighboring buildings presence, since the turbines are situated closer in this position. By comparing averaged power-changes in all the examined positions for the *low* and the *high* turbine, they are in agreement with findings by (Hakimi and Lubitz, 2016). They reported on the effect of wind directions over a peaked roof-building in an urban environment, that the greatest variations in the wind speeds are found closest to the roof over the sweep. Since the *low* turbine operates closer to the roof, it can explain why the biggest average power-change are seen for the *low* turbine in table 3.

By studying the average power-gains and losses with respect to the "clean air" benchmark test in table 3, it can be seen that independent of the method and the turbine, the optimal position to mount the turbine is at position 2, representing the center of the building. Here, the *high* turbine thrives and gains more than 20% by standing on the roof instead of in the free-stream. From fig. 10, it is apparent that it performs particularly well at $\theta = 90°$ and $\theta = 105°$ which is expected since it is situated closer to the wind passage between the modeled buildings where the flow is accelerated. Moreover, an interesting results is that position 3 was deemed the worst position from the data in table 2 and similar was found in Jooss et al. (2021), yet, here it shows that it is rather close to be the most suitable spot to site a

14

turbine besides position 2. Furthermore, a special notice could be pointed at position 1 which was found most optimum in Jooss et al. (2021) when they considered only one inflow angle, yet, here it shows less advantage than being in the free-stream with an average power-loss of 1.1%. Hence, to truly acquire a realistic performance assessment in the urban environment, one should not draw conclusions on favourable wind directions and the power measurements at these inflow angles, but rather state the average power yield. One might deem the *low* turbine insufficient for an energy harvesting purpose on the roof since it could not achieve any great advantages at the examined positions. On the contrary, the *high* turbine is the superior turbine for which have great gains by standing on the roof. These results are thereby showing how a slight change in the turbine elevation above the roof can increase the performance drastically.

Table 3: Turbine site analysis. Method A - the averaged maximum performance $\overline{C_{P_{max}}}$ obtained in the power curves collected from table 2, denoted $\overline{C_{P_{pc}}}$. Method B - the averaged performance from the angle-sweep in fig. 10, denoted $\overline{C_{P_{as}}}$. Method C - the averaged maximum performance by combining the optimal data-points, given as $\overline{C_{P_{pc+as}}}$. In addition, $(\overline{C_{P_{pc+as}}}/\overline{C_{P_{pc}}})-1$ refers to the change in performance by having a finer inflow angle discretization. Lastly, the averaged gains and losses in power by placing the turbine on the roof, with respect to the yield in "clean air" from section 4.1. Like table 2, both values of $C_{P_{ca}}$ are used as reference. Here, the green and red colors denoting gains and losses, respectively. The dark-green highlights the greatest gains.

Turbine	Position	Method A: Power curves $\overline{C_{P_{pc}}}$	Method B: Angle sweep $\overline{C_{P_{as}}}$	Method C: Combination $\overline{C_{P_{pc+as}}}$	Clean air $\overline{C_{P_{ca}}}$	$(\overline{C_{P_{pc+as}}}/\overline{C_{P_{pc}}})-1$	$(\overline{C_{P_{pc+as}}}/\overline{C_{P_{ca}}})-1$
Low	1	0.037	0.040	0.042	0.042	13.9%	-1.1%
	2	0.039	0.041	0.044	0.042	13.6%	3.6%
	3	0.034	0.0403	0.044	0.042	28.5%	3.1%
High	1	0.042	0.043	0.046	0.042	9.4%	12.2%
	2	0.048	0.048	0.050	0.042	5.7%	20.6%
	3	0.043	0.0467	0.050	0.042	17.2%	20.3%

5 Conclusions

Power measurements of a scaled-down Savonius wind turbine mounted on the roof over two cubes in tandem arrangement with two cube-height spacing were carried out experimentally in the wind tunnel. A parametric study was conducted with the aim to identify the ideal turbine position. The following parameters were under investigation: two equally-designed turbines with different elevation above the roof denoted *high* and *low*, thirteen wind directions and three sites on the roof. The sites were numbered position 1, 2 and 3 corresponding to the front, center and the far back of the cube, respectively. The set-up was designed based on a previous study by Jooss et al. (2021) while allowing different incoming wind directions by rotating the system. The power was examined by obtaining data on the estimated mechanical torque and the rotational velocity. As a reference, the power was measured in a "clean air" configuration with the cubes removed, denoted $C_{P_{ca}}$. To obtain information on the flow field, pressure was measured on the cubes surfaces and the pressure on the roof was found to be similar to the previous study by Castro and Robins (1977). It has been shown in the present study that the influence of a neighbouring modeled building is immense which was reflected in the power measurements and the pressure fields. Moreover, the incoming wind angle was decisive for the power output. Hence, to obtain an estimate of the optimal turbine site, the measurements were carried out over the full rotation and the average maximum power $\overline{C_{P_{max}}}$ was reported at each of the investigated positions. Out of two turbine heights investigated, the *high* turbine was the favourable one. With the blade swept area at $1.16 \leq z/H \leq 1.48$, the achieved performance was shown to be better than that of reference $\overline{C_{P_{ca}}}$ on an overall average basis, yielding 12.2%, 20.6% and 20.3% in position 1, 2 and 3, respectively. The *low* turbine was not equally efficient. Still, it surpassed the *high* turbine for some specific wind directions. The reason for why the low turbine performed particularly well at $\theta = 45°$ was explained with the mean stream-wise velocities obtained by Castro and Robins (1977) on a stand-alone cube. Furthermore, independent of the turbine height, the best performance can be achieved in position 2, yet, position 3 is almost equally ideal to site a turbine. The *high* turbine was found to be less influenced by the incoming wind angle on average than

the *low* turbine. Moreover, the favourable wind directions ($\theta = 90°$ and $105°$ for the *high* turbine) were pointed out. The gain in power at these inflow angles can be explained by the accelerated flow in the cube passage, which is indicated in the pressure fields. Both the present study and the data by Jooss et al. (2021) show the optimal site to be in position 1 as $\theta = 0°$, however, the results changed considerably when the average power over the full rotation was considered, with losses of 1.1% for position 1 compared to the benchmark test in "clean air", $\overline{C_{P_{ca}}}$. Due to the fact that the performance is enhanced by up to more than 20% by mounting the turbines on the roof, the present study suggests an overall positive outlook for urban wind energy. Future studies should explore the effects of different spacing as the neighbouring cube showed great impact on the performance. It would also be interesting to see the effects of adjusting the elevated turbine height further since the power was found to be sensitive to this.

References

I. Abohela, N. Hamza, and S. Dudek. Effect of roof shape, wind direction, building height and urban configuration on the energy yield and positioning of roof mounted wind turbines. *Renewable Energy*, 50:1106–1118, Feb. 2013. ISSN 0960-1481. doi: 10.1016/j.renene.2012.08.068.

J. V. Akwa, H. A. Vielmo, and A. P. Petry. A review on the performance of Savonius wind turbines. *Renewable and Sustainable Energy Reviews*, 16(5):3054–3064, June 2012. ISSN 1364-0321. doi: 10.1016/j.rser.2012.02.056.

A. Al-Quraan, T. Stathopoulos, and P. Pillay. Comparison of wind tunnel and on site measurements for urban wind energy estimation of potential yield. *Journal of Wind Engineering and Industrial Aerodynamics*, 158:1–10, 2016. ISSN 0167-6105. doi: https://doi.org/10.1016/j.jweia.2016.08.011.

A. D. Aliferis, M. S. Jessen, T. Bracchi, and R. J. Hearst. Performance and wake of a Savonius vertical-axis wind turbine under different incoming conditions. *Wind Energy*, 22(9):1260–1273, 2019. ISSN 1099-1824. doi: https://doi.org/10.1002/we.2358.

A. Amer, A. Azab, M. A. Azzouz, and A. S. Awad. A stochastic program for siting and sizing fast charging stations and small wind turbines in urban areas. *IEEE Transactions on Sustainable Energy*, 12(2):1217–1228, 2021.

D. Banks, R. Meroney, P. Sarkar, Z. Zhao, and F. Wu. Flow visualization of conical vortices on flat roofs with simultaneous surface pressure measurement. *Journal of Wind Engineering and Industrial Aerodynamics*, 84(1):65–85, 2000.

M. Bastankhah and F. Porté-Agel. A New Miniature Wind Turbine for Wind Tunnel Experiments. Part I: Design and Performance. *Energies*, 10(7):908, July 2017. doi: 10.3390/en10070908.

B. F. Blackwell, L. V. Feltz, and R. E. Sheldahl. *Wind tunnel performance data for two-and three-bucket Savonius rotors*. Sandia Laboratories Albuquerque, New Mexico, 1977.

B. Blocken, P. Moonen, T. Stathopoulos, and J. Carmeliet. Numerical study on the existence of the venturi effect in passages between perpendicular buildings. *Journal of engineering mechanics*, 134(12):1021–1028, 2008.

J. Bukala, K. Damaziak, K. Kroszczynski, M. Krzeszowiec, and J. Malachowski. Investigation of parameters influencing the efficiency of small wind turbines. *Journal of Wind Engineering and Industrial Aerodynamics*, 146:29–38, 2015. ISSN 0167-6105. doi: https://doi.org/10.1016/j.jweia.2015.06.017.

T. Burton, D. Sharpe, N. Jenkins, and E. Bossanyi. *Wind energy handbook*, volume 2. Wiley Online Library, 2001.

J. J. C. G. Cantan. The effect of active grid-generated freestream turbulence on an aeroelastic NACA4412 airfoil. Master's thesis, Norges teknisk-naturvitenskapelige universitet, 2021.

P. Case and N. Isyumov. Wind loads on low buildings with 4: 12 gable roofs in open country and suburban exposures. *Journal of Wind Engineering and Industrial Aerodynamics*, 77:107–118, 1998.

I. P. Castro and A. G. Robins. The flow around a surface-mounted cube in uniform and turbulent streams. *Journal of Fluid Mechanics*, 79(2):307–335, Feb. 1977. ISSN 1469-7645, 0022-1120. doi: 10.1017/S0022112077000172.

S. Chapman. *Electric machinery fundamentals*. Tata McGraw-Hill Education, 2005.

H. W. Coleman and W. G. Steele. *Experimentation, validation, and uncertainty analysis for engineers*. John Wiley & Sons, 2018.

W. Colglazier. Sustainable development agenda: 2030. *Science*, 349(6252):1048–1050, 2015.

S. de Jong Helvig, M. K. Vinnes, A. Segalini, N. A. Worth, and R. J. Hearst. A comparison of lab-scale free rotating wind turbines and actuator disks. *Journal of Wind Engineering and Industrial Aerodynamics*, 209:104485, 2021.

W. El-Askary, M. Nasef, A. AbdEL-hamid, and H. Gad. Harvesting wind energy for improving performance of savonius rotor. *Journal of Wind Engineering and Industrial Aerodynamics*, 139:8–15, 2015. ISSN 0167-6105. doi: https://doi.org/10.1016/j.jweia.2015.01.003.

S. Franchini, S. Pindado, J. Meseguer, and A. Sanz-Andrés. A parametric, experimental analysis of conical vortices on curved roofs of low-rise buildings. *Journal of Wind Engineering and Industrial Aerodynamics*, 93(8):639–650, 2005.

S. Gambuzza and B. Ganapathisubramani. The effects of free-stream turbulence on the performance of a model wind turbine. *Journal of Renewable and Sustainable Energy*, 13(2):023304, Mar. 2021. doi: 10.1063/5.0039168. Publisher: American Institute of Physics.

M. Ge, D. F. Gayme, and C. Meneveau. Large-eddy simulation of wind turbines immersed in the wake of a cube-shaped building. *Renewable Energy*, 163:1063–1077, 2021. ISSN 0960-1481. doi: 10.1016/j.renene.2020.08.156.

B. Grieser, Y. Sunak, and R. Madlener. Economics of small wind turbines in urban settings: An empirical investigation for Germany. *Renewable Energy*, 78:334–350, 2015. ISSN 0960-1481. doi: https://doi.org/10.1016/j.renene.2015.01.008.

R. Hakimi and W. D. Lubitz. Wind environment at a roof-mounted wind turbine on a peaked roof building. *International Journal of Sustainable Energy*, 35(2):172–189, 2016.

R. J. Hearst, G. Gomit, and B. Ganapathisubramani. Effect of turbulence on the wake of a wall-mounted cube. *Journal of Fluid Mechanics*, 804:513–530, Oct. 2016. ISSN 0022-1120, 1469-7645. doi: 10.1017/jfm.2016.565.

H. Hemida, A. Šarkić Glumac, G. Vita, K. Kostadinović Vranešević, and R. Höffer. On the Flow over High-rise Building for Wind Energy Harvesting: An Experimental Investigation of Wind Speed and Surface Pressure. *Applied Sciences*, 10(15):5283, Jan. 2020. doi: 10.3390/app10155283. Number: 15 Publisher: Multidisciplinary Digital Publishing Institute.

A. Hughes and B. Drury. *Electric motors and drives: fundamentals, types and applications*. Newnes, 2019.

Y. Jooss, R. Bolis., T. Bracchi., and R. J. Hearst. Flow field and performance of a vertical axis wind turbine on model buildings. *Flow*, page 1–17, 2021. Under review.

H. S. Kang and C. Meneveau. Direct mechanical torque sensor for model wind turbines. *Measurement Science and Technology*, 21(10):105206, 2010.

S. Kooiman and S. Tullis. Response of a Vertical Axis Wind Turbine to Time Varying Wind Conditions Found within the Urban Environment. *Wind Engineering*, 34(4):389–401, June 2010. ISSN 0309-524X. doi: 10.1260/0309-524X.34.4.389. Publisher: SAGE Publications.

H. Landau. Sampling, data transmission, and the nyquist rate. *Proceedings of the IEEE*, 55(10):1701–1706, 1967.

L. Ledo, P. B. Kosasih, and P. Cooper. Roof mounting site analysis for micro-wind turbines. *Renewable Energy*, 36(5):1379–1391, May 2011. ISSN 0960-1481. doi: 10.1016/j.renene.2010.10.030.

K.-Y. Lee, S.-H. Tsao, C.-W. Tzeng, and H.-J. Lin. Influence of the vertical wind and wind direction on the power output of a small vertical-axis wind turbine installed on the rooftop of a building. *Applied Energy*, 209:383–391, 2018. ISSN 0306-2619. doi: https://doi.org/10.1016/j.apenergy.2017.08.185.

J.-X. Lin, D. Surry, and H. Tieleman. The distribution of pressure near roof corners of flat roof low buildings. *Journal of wind engineering and industrial aerodynamics*, 56(2-3):235–265, 1995.

L. Lu and K. Y. Ip. Investigation on the feasibility and enhancement methods of wind power utilization in high-rise buildings of hong kong. *Renewable and Sustainable Energy Reviews*, 13(2):450–461, 2009. ISSN 1364-0321. doi: https://doi.org/10.1016/j.rser.2007.11.013.

J. F. Manwell, J. G. McGowan, and A. L. Rogers. *Wind energy explained: theory, design and application.* John Wiley & Sons, 2010.

R. J. Martinuzzi and B. Havel. Turbulent Flow Around Two Interfering Surface-Mounted Cubic Obstacles in Tandem Arrangement. *Journal of Fluids Engineering*, 122(1):24, 2000. ISSN 00982202. doi: 10.1115/1.483222.

R. J. Martinuzzi and B. Havel. Vortex shedding from two surface-mounted cubes in tandem. *International Journal of Heat and Fluid Flow*, 25(3):364–372, June 2004. ISSN 0142-727X. doi: 10.1016/j.ijheatfluidflow.2004.02.003.

S. Mertens. The Energy Yield of Roof Mounted Wind Turbines. *Wind Engineering*, 27(6):507–518, Dec. 2003. ISSN 0309-524X. doi: 10.1260/030952403773617472. Publisher: SAGE Publications.

S. Mertens, G. van Kuik, and G. van Bussel. Performance of an h-darrieus in the skewed flow on a roof. *J. Sol. Energy Eng.*, 125(4):433–440, 2003.

M. Mohamed, G. Janiga, E. Pap, and D. Thévenin. Optimal blade shape of a modified savonius turbine using an obstacle shielding the returning blade. *Energy Conversion and Management*, 52(1):236–242, 2011.

Y. Ogawa, S. Oikawa, and K. Uehara. Field and wind tunnel study of the flow and diffusion around a model cube—i. flow measurements. *Atmospheric Environment (1967)*, 17(6):1145–1159, 1983.

T. Oke. The urban energy balance. *Progress in Physical Geography: Earth and Environment*, 12(4):471–508, Dec. 1988. ISSN 0309-1333. doi: 10.1177/030913338801200401. Publisher: SAGE Publications Ltd.

M. R. Raupach, R. A. Antonia, and S. Rajagopalan. Rough-Wall Turbulent Boundary Layers. *Applied Mechanics Reviews*, 44(1):1–25, Jan. 1991. ISSN 0003-6900. doi: 10.1115/1.3119492.

P. Richards, R. Hoxey, B. Connell, and D. Lander. Wind-tunnel modelling of the Silsoe cube. *Journal of Wind Engineering and Industrial Aerodynamics*, 95(9):1384–1399, 2007. ISSN 0167-6105. doi: https://doi.org/10.1016/j.jweia.2007.02.005.

T. Stathopoulos, H. Alrawashdeh, A. Al-Quraan, B. Blocken, A. Dilimulati, M. Paraschivoiu, and P. Pilay. Urban wind energy: Some views on potential and challenges. *Journal of Wind Engineering and Industrial Aerodynamics*, 179:146–157, Aug. 2018. ISSN 0167-6105. doi: 10.1016/j.jweia.2018.05.018.

F. Toja-Silva, A. Colmenar-Santos, and M. Castro-Gil. Urban wind energy exploitation systems: Behaviour under multidirectional flow conditions—opportunities and challenges. *Renewable and Sustainable Energy Reviews*, 24:364–378, 2013. ISSN 1364-0321. doi: https://doi.org/10.1016/j.rser.2013.03.052.

F. Toja-Silva, C. Peralta, O. Lopez-Garcia, J. Navarro, and I. Cruz. Roof region dependent wind potential assessment with different RANS turbulence models. *Journal of Wind Engineering and Industrial Aerodynamics*, 142:258–271, 2015.

F. Toja-Silva, T. Kono, C. Peralta, O. Lopez-Garcia, and J. Chen. A review of computational fluid dynamics CFD simulations of the wind flow around buildings for urban wind energy exploitation. *Journal of Wind Engineering and Industrial Aerodynamics*, 180:66–87, 2018. ISSN 0167-6105. doi: https://doi.org/10.1016/j.jweia.2018.07.010.

Ultimaker. Ultimaker S5 accuracy. https://ultimaker.com/3d-printers/ultimaker-s5. Accessed: 2021-06-18.

A. Á. Vilar, G. Xydis, and E. A. Nanaki. Small wind: a review of challenges and opportunities. *Sustaining Resources for Tomorrow*, pages 185–204, 2020.

R. Wagner, I. Antoniou, S. M. Pedersen, M. S. Courtney, and H. E. Jørgensen. The influence of the wind speed profile on wind turbine performance measurements. *Wind Energy*, 12(4):348–362, 2009. ISSN 1099-1824. doi: 10.1002/we.297.

B. Wang. Urban wind energy evaluation with urban morphology. *Modeling, Simulation and Optimization of Wind Farms and Hybrid Systems*, page 101, 2020.

B. Wang, L. Cot, L. Adolphe, and S. Geoffroy. Estimation of wind energy of a building with canopy roof. *Sustainable Cities and Society*, 35:402–416, 2017. ISSN 2210-6707. doi: https://doi.org/10.1016/j.scs.2017.08.026.

G. S. West and C. J. Apelt. The effects of tunnel blockage and aspect ratio on the mean flow past a circular cylinder with Reynolds numbers between 104 and 105. *Journal of Fluid Mechanics*, 114:361–377, Jan. 1982. ISSN 1469-7645, 0022-1120. doi: 10.1017/S0022112082000202. Publisher: Cambridge University Press.

A. J. Wheeler and A. R. Ganji. *Introduction to engineering experimentation*, volume 199. Prentice Hall New Jersey, 1996.

A. Šarkić Glumac, H. Hemida, and R. Höffer. Wind energy potential above a high-rise building influenced by neighboring buildings: An experimental investigation. *Journal of Wind Engineering and Industrial Aerodynamics*, 175:32–42, 2018. ISSN 0167-6105. doi: https://doi.org/10.1016/j.jweia.2018.01.022.

Appendices

A   Figures, tables and equations

A.1   Fixed tip-speed ratio

The other approach to obtain near-optimum data-points carried out over the sweep in section 4.3 was keeping λ fixed. Even though λ is not optimal generally speaking, it has been included to discuss the problem at hand. It was chosen based on the respective value of the maximum power in the "clean air", seen in fig. 8. However, by keeping $\lambda = 0.346 \pm 0.01$ it can not be optimal for all the inflow angles tested since the curves are shifted to the right for higher local mean velocities and opposite for lower local mean velocities. This can be seen by looking at the reported values of λ in table 2. Here, the fixed value is too low examining the *high* turbine suggesting as much as $\lambda > 0.45$ at the favourable wind conditions. Moreover, by considering the other side of the scale, the optimal tip-speed ratio for the *low* turbine are far lower and since position 3 in fig. 9 does not span this demanded λ-value due to its poor flow conditions, no lambda greater than 0.28 was possible to achieve. The values of λ together with the performance measurements over the sweep, are shown in section A.1.
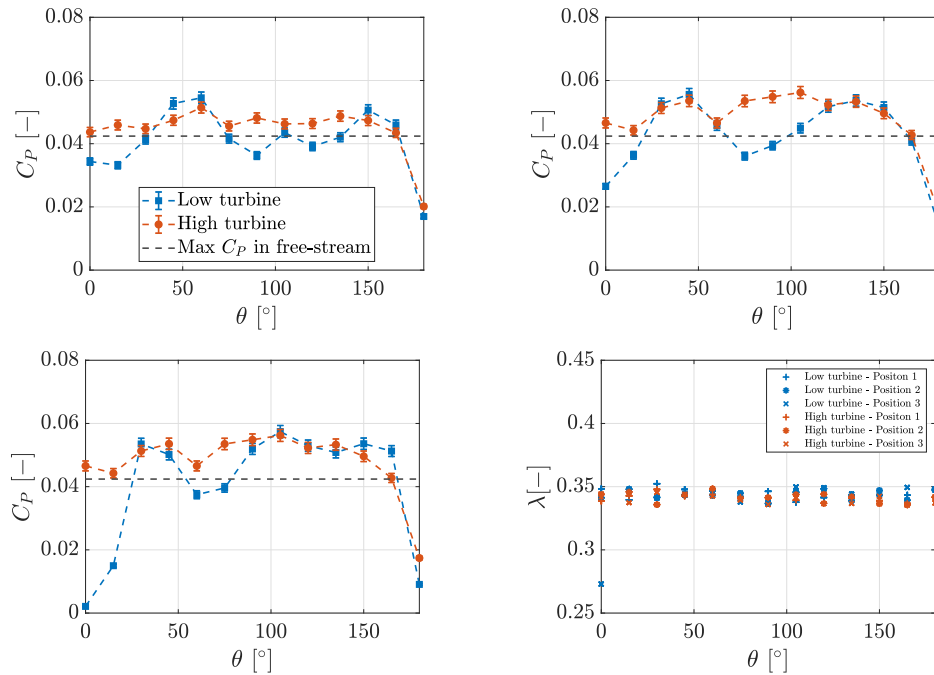

Figure 11: Fixed tip-speed ratio, $\lambda = 0.346 \pm 0.01$

It can be seen that the results are relatively similar to the results based on the fixed-k approach in fig. 10. Still, the tip-speed ratio value that were optimal for "clean air", is too low to extract the maximum power over the roof, especially seen for the *high* turbine in position 2 and 3.

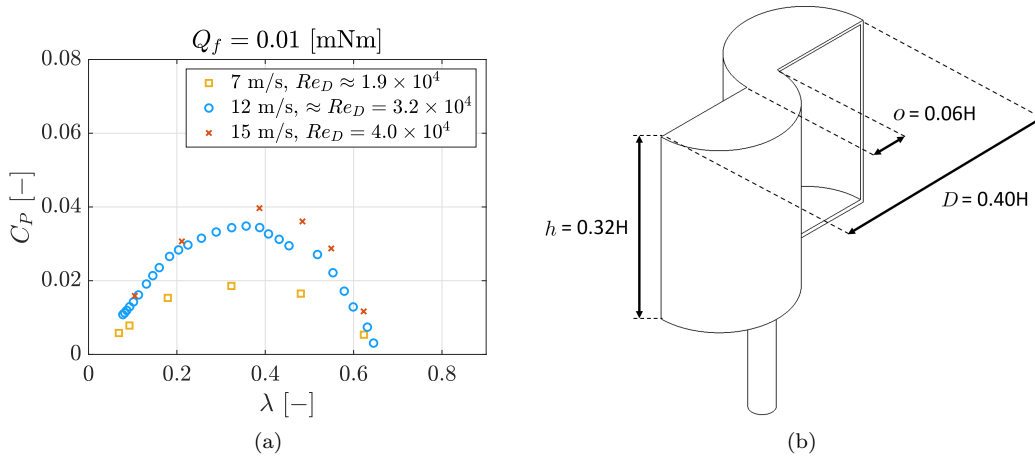## A.2 Reynolds dependence and the savonius turbine model

Figure 12: (a) Distinct Reynolds effects can be seen on the Savonius wind turbine when placed in an open wind tunnel provided by GUNT with a test section area of 0.292 m × 0.292 m (see fig. 13(c)). The performance is calculated based on a fixed velocity read by an incline tube manometer, which has been shown to be in good agreement with pitot-static tube measurements beforehand. All the data-points for each curve are based on the same velocity and density. The friction torque used is given in the title. Moreover, it should be mentioned that blockage is not corrected for as well as other open holes in the tunnel are not covered (see fig. 13(c)). Furthermore, the tower beneath and the turbine's tower-height were different in this analysis than in the closed loop tunnel experiments. From the figure, the trends are conserved and it is visible that increasing the Reynolds number increases the turbine performance. (b) The Savonius two-bucket rotor used in the experiments. The bucket overlap, $o = 0.06H$, is shown together with the height $h = 0.32H$ and diameter $D = 0.4H0$.

A.3 Uncertainties

The uncertainties are calculated as in Wheeler and Ganji (1996); let the result R be a function of n measured variables x_n and dependent only on the product of the variables, that is: $R = Cx_1^a x_2^b \ldots x_n^N$, where C is a constant, the maximum total uncertainty σ_R in R is by the law of error propagation given by:

$$\sigma_R = R\sqrt{\left(a\frac{\sigma_1}{x_1}\right)^2 + \left(b\frac{\sigma_2}{x_2}\right)^2 + \cdots + \left(N\frac{\sigma_n}{x_n}\right)^2} \tag{3}$$

where $\sigma_1/x_1, \sigma_2/x_2, \ldots \sigma_n/x_n$ are the relative error of the root sum square of the biased and the random error in variables $x_1, x_2, \ldots x_n$, respectively. The correlation terms are left out by assuming the measured quantities are independent of each other (Coleman and Steele (2018)). Applying this procedure to C_P (1) and the tip-speed ratio $\lambda = \Omega R/U_\infty$, the averaged uncertainties in the power performances were mapped based on data calculated for a 95% confidence interval.

While the calculated random uncertainty in U_∞ is found negligible over long time-samples, the biased error originating from the pitot-tube and the portable calibrator and precision manometer, FCO560, are of significance having 0.5% and 0.1% error, respectively. Air density ρ_∞ was found based on the ideal gas law assumption, $\rho_\infty = p_{atm}/RT_\infty$, where R is the specific gas constant of air and T_∞ is the temperature measured with a type K thermocouple. Uncertainties in the read atmospheric pressure (0.01%) air temperature (0.75%) are accounted for, unlike that of the swept turbine-area, A, which can be neglected since the Ultimaker 3D-printer of type S5 is said to have great precision by the manufacturer, where they report a layer resolution of 20 micron= 0.02 mm and a XYZ resolution of 2.5 micron (Ultimaker). Even though the aforementioned random uncertainties are found relatively negligible in comparison with their systematic errors, it was not the case for Ω. Here, even for two-minute-long samples, including a 0.4%

"worst case"-error for counted rounds missed by the optical sensor during the sample period, the total error was calculated to 1.1%.

The mechanical torque Q_{mech} is a function of three parameters; I, k_M and Q_f, for which statistical random errors were found of significance for I (0.5%) and the biased maximum gained error for the INA219 sensor is said to be 0.5%. Furthermore, the manufacturer-provided torque constant k_M may be inaccurately measured, however, this uncertainty is unknown and not accounted for in this analysis. In addition, a constant friction torque of $Q_f = 0.01$ mNm was used in the measurements, underestimating the supported data from the specification sheet T_f (seen in table 1) by a factor of eight. This was initially decided based on a parameter-analysis carried out in the prefatory phase, which showed extreme rates of C_P for low values of λ. This was solely due to the huge relative friction power, P_f/P. Hence, using T_f rather than an estimated torque-friction quantity, Q_f, would propose incorrect performance-values for lower rotational velocities. However, despite choosing another friction torque constant, the exact value is not important if the trends are conserved, which they were. The friction is also found by Bastankhah and Porté-Agel (2017) to decrease when the motor, used as a generator, start spinning at slower speeds. A possible explanation for the large quoted value of T_f is found by looking at the differences in normal speed-range of the debated PMDC machine (see table 1). Due to big changes in the parameters stated above, the error-calculation was finally based on the assumption of Q_{mech} being exclusively dependent of I. All values aforementioned are included in the error-bars.

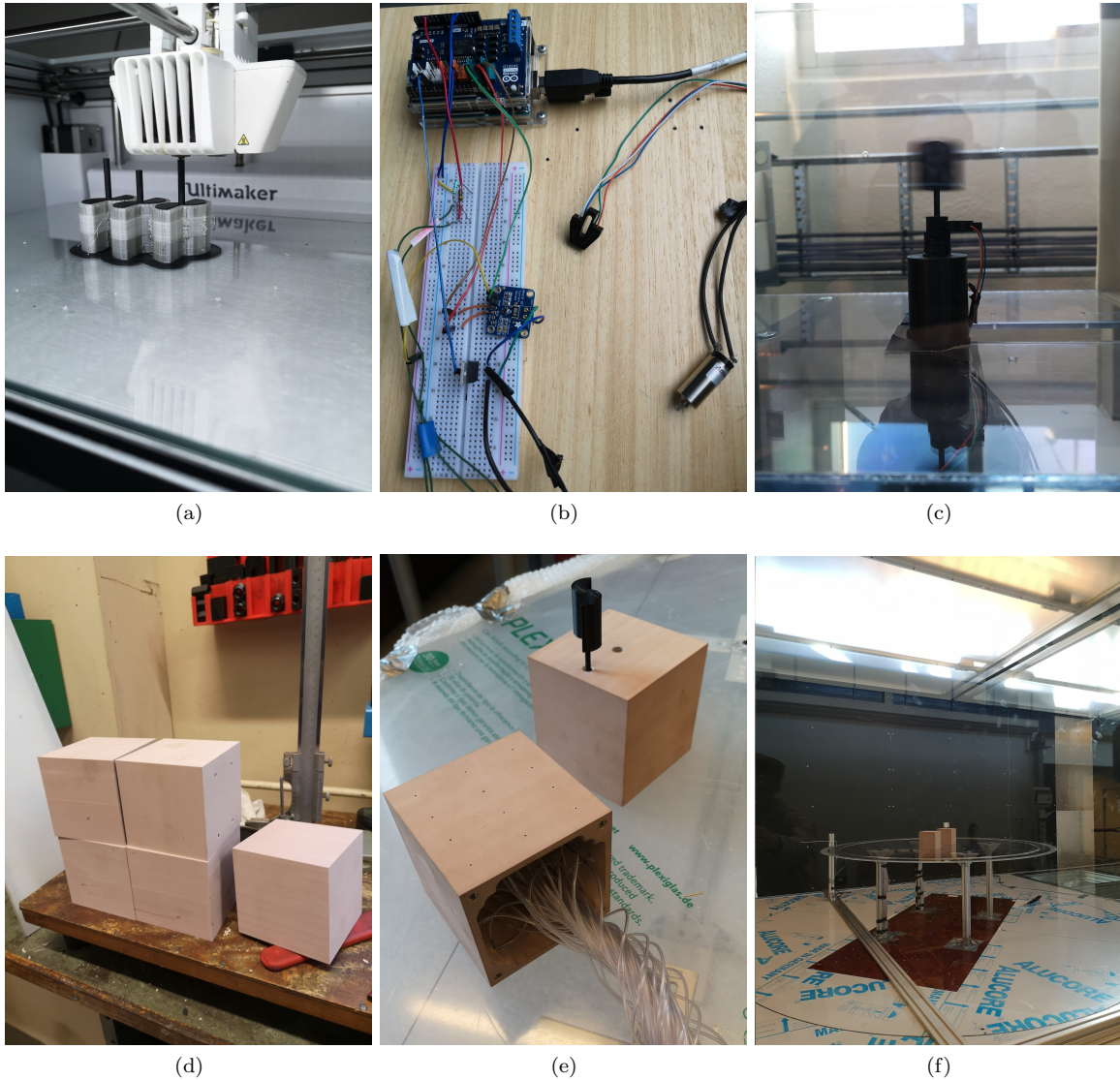# B   Experimental set-up and model construction

Figure 13: Pictures of the components and the course of events on the construction of the model. (a) The Ultimaker 3D-printer of type S5 under an operation. The material used for the turbines was PLA whereas PVA was usedas fill-material for support. (b) The electrical components and the breadboard used in the experiments. (c) The turbine was tested in an open wind tunnel in the prefatory phase were the effects of low Reynolds numbers were found of significance by adjusting velocity U_∞. (d) The cubes made of Ebaboard 0600 were cut by a technician and shaped exact. (e) The cubes were later hollowed to make space for the motor used as a generator as well as the tubes for the pressure taps. (f) Fully-assembled model inside the wind tunnel. The pitot tube was placed next to the plate. Wires were hidden to avoid flow obstructions on the sharp acrylic plate and the 2 mm metal rod used to trip the boundary layer can be seen. The rotating plate gives in this present orientation an inflow angle of $\theta = 135°$.